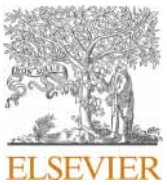
Nano Energy 156 (2026) 112134



Contents lists available at ScienceDirect

Nano Energy

journal homepage: www.elsevier.com/locate/nanoen



Full Paper



Electrostatic tweezers enabling programmable, non-contact control of charged membranes

Lixue Yang [a,b], Ziyang Wang [c], Zunkang Zhou [a,d], Yu Wei [a,d], Jie Fu [e], Zhongqiang Zhang [c,f,*], Zhe Wang [b,g,h,**], Zhong Lin Wang [a,***], Di Wei [a,i,****]

[a] Beijing Institute of Nanoenergy and Nanosystems, Chinese Academy of Sciences, Beijing 101400, China
[b] School of Chemistry and Life Sciences, Changchun University of Technology, Changchun 130012, China
[c] Institute of Intelligent Flexible Mechatronics, Jiangsu University, Zhenjiang 212013, China
[d] School of Nanoscience and Engineering, University of Chinese Academy of Sciences, Beijing 100049, China
[e] Zhejiang Wansheng co., ltd No.8, Jujing Rd. Liangshui Development Zone, Linhai, Zhejiang, China
[f] State Key Laboratory of Struchural Analysis for Industrial Equipment, Department of Einginering Mechanic, Faculy of Vehicle Einginering and Mechanics, Dalian University of Technology, Dalian 116024, China
[g] Advanced Institute of Materials Science, Changchun University of Technology, Changchun 130012, China
[h] Key Laboratory of Advanced Functional Polymer Membrane Materials of Jilin Province, Changchun 130012, China
[i] Centre for Photonic Devices and Sensors, University of Cambridge, 9 JJ Thomson Avenue, Cambridge CB3 0FA, UK

ARTICLE INFO

Keywords:
Electrostatic tweezers
Charged membranes
Non-contact control
Covalent organic framework (COF)

ABSTRACT

Remote, contact-free manipulation of solid matter remains a central challenge for materials transport, soft actuation and reconfigurable systems. Existing non-contact approaches based on optical, magnetic, ultrasonic or photothermal mechanisms are often constrained by environmental sensitivity, rigid device architectures or limited material compatibility. Here we introduce an electrostatic tweezer (ET) that enables remote, omnidirectional, through-air electrostatic actuation of charged membranes at air-liquid interfaces. As a model system, a charged covalent organic framework (COF) membrane constructed from tri (4-aminophenyl) amine (TAPA) and 2,4,6-triformylresorcinol (TFP) exhibits rapid and programmable motion under electrostatic field, operating without external bias, electrodes or electrode patterning. The membrane floats on a thin water layer that provides buoyancy and reduces interfacial friction, enabling sensitive response to weak electrostatic forces. In contrast to conventional electrostatic actuation, which is largely restricted to droplet-based systems, this approach enables programmable trajectory control for remote actuation of charged membranes, with a 5 mm $\times$ 5 mm TAPA-TFP membrane reaching a peak velocity of about 10 mm s^{-1} under electrostatic charging conditions. The ET maintains stable performance across wide ranges of temperature, humidity, surface chemistry and electrolyte composition, in agreement with COMSOL simulations, enabling two- and three-dimensional omnidirectional manipulation, uphill motion on inclined surfaces, selective control, metamorphic origami remote transformations and load-coupled actuation. This work establishes a fundamentally new paradigm for the remote, contact-free manipulation of charged membranes, demonstrating that electrostatic fields can be harnessed to achieve programmable motion, metamorphic origami remote control and load-bearing transport of charged membranes, capabilities that remain inaccessible to existing non-contact manipulation technologies.

1. Introduction

Contact-free remote manipulation is a foundational capability for industrial automation [1,2], precision manufacturing [3,4], biomedicine [5,6], and biopharmaceutical processing [7,8], enabling high-accuracy operations in hazardous, enclosed, or contamination-sensitive environments while avoiding mechanical damage and cross-contamination [9,10]. Existing non-contact

* Corresponding author at: Institute of Intelligent Flexible Mechatronics, Jiangsu University, Zhenjiang 212013, China.
** Corresponding author at: School of Chemistry and Life Sciences, Changchun University of Technology, Changchun 130012, China.
*** Corresponding author.
**** Corresponding author at: Beijing Institute of Nanoenergy and Nanosystems, Chinese Academy of Sciences, Beijing 101400, China.
E-mail addresses: zhangzq@ujs.edu.cn (Z. Zhang), wangzhe@ccut.edu.cn (Z. Wang), zlwang@binn.cas.cn (Z.L. Wang), weidi@binn.cas.cn (D. Wei).

https://doi.org/10.1016/j.nanoen.2026.112134
Received 13 May 2026; Received in revised form 9 June 2026; Accepted 16 June 2026
Available online 18 June 2026
2211-2855/© 2026 Elsevier Ltd. All rights are reserved, including those for text and data mining, AI training, and similar technologies.

manipulation technologies, including ultrasonic [11], optical [12], magnetic [13,14], and photothermal [15,16] approaches, have enabled impressive advances in droplet and microscale object control. However, each modality is intrinsically constrained, ultrasonic actuation is highly sensitive to media and boundary conditions [17,18], optical tweezers are restricted to microscopic particles [19], magnetic control requires magnetically responsive targets [13,14], and photothermal [15,16] methods depend strongly on material properties and environmental stability. Electric-based manipulation offers distinct advantages in cost, response speed, directional programmability, and environmental adaptability [20–22], yet the dominant electrowetting-on-dielectric (EWOD) paradigm relies on complex electrode arrays and external power sources, limiting flexibility, scalability, safety, and portability [23–26]. Moreover, EWOD is inherently confined to fluidic systems and remains fundamentally incompatible with macroscopic solids in open aqueous environments [22,27,28].

Electrostatic control techniques offer a promising alternative to overcome the aforementioned limitations [29–33]. Different from EWOD, it operates by regulating the surface charges between materials and the resulting electric field distribution. This mechanism enables the contact-free mechanical actuation of objects across a wide range of scales and requires no complex electrode arrays or external power sources. Instead, it relies solely on electrostatic field to generate stable and appreciable electrostatic forces in open environments, enabling attraction, repulsion, gripping and directional transport of micro/-nanoparticles, droplets and biological objects in air, on interfaces or in confined spaces. Recent advancements include charge-induced directional propulsion of droplets on superhydrophobic surfaces, self-powered electrostatic tweezers that use triboelectric charges to accomplish multistep microfluidic operations such as splitting, fusion, mixing, and transport, as well as open microfluidic systems that achieve droplet sequencing, temporal regulation, and logic operations through induced charges [21,32–34]. Despite remarkable progress, nearly all existing electrostatic manipulation strategies remain restricted to droplet manipulation.

By contrast, remote manipulation of solid materials represents a far more powerful and technologically consequential frontier. Unlike droplets, solid materials combine geometric stability with programmable mechanical, electrical, optical, and chemical functionality, enabling complex tasks such as grasping, assembly, cargo transport, and structural reconfiguration [35–38]. Their robustness allows stable operation under extreme conditions without evaporation, shape collapse, or chemical degradation, while enabling submicron precision and long-term positional stability [39–42]. Moreover, solid materials can integrate catalysts, electronic components, or bioactive agents, supporting applications ranging from micro-nano device assembly and microrobotic drug delivery to environmental sensing and space deployment [43–47]. Achieving non-contact, remotely programmable manipulation of macroscopic solids therefore represents a critical unmet challenge with broad implications for intelligent manufacturing, soft robotics, micro/nano engineering, and biomedical systems [48,49].

Here, we report a previously unexplored electrostatic tweezer (ET) that harnesses electrostatic fields to enable remote, omnidirectional through-air electrostatic actuation of charged membranes at air-liquid interfaces without external power sources or complex electrode architectures. In conventional tweezers, objects are manipulated through applied force fields, whereas ETs achieve manipulation by harnessing electrostatic fields. In this context, the electrostatic field used in ET is functionally equivalent to the force field in traditional tweezers, meaning that any material capable of generating an electrostatic field can act as the actuation source. Charged TAPA-TFP polymer membranes, constructed from tri (4-aminophenyl) amine (TAPA) and 2,4,6-triformylresorcinol (TFP), respond to electric fields generated by external materials (nylon film/polytetrafluoroethylene film (PTFE)) enabling rapid and programmable motion and along arbitrary trajectories. In contrast to prior electrostatic strategies confined to droplets, the ET extends actuation to charged membranes, enabling directional transport in enclosed environments and active payload delivery. The ET operates across a wide range of conditions, including membrane sizes from 5 mm × 5 mm to 10 mm × 10 mm, broad temperature (from room temperature to 200 ℃) and humidity (RH 20–95%) ranges, diverse surface chemical states, and various electrolyte compositions and concentrations. It supports two-dimensional (2D) and three-dimensional (3D) pathway movement, uphill motion on inclined surfaces, selective manipulation based on surface chemistry, agile direction steering, and fully programmable transport pathways. The platform is equally effective in open aqueous environments and enclosed systems, enabling metamorphic origami remote control, and load-coupled transport with high reproducibility, rapid response, and long-term stability. Together, the ET establishes a new paradigm for non-contact electrostatic manipulation of charged membranes, bridging a critical gap between electrostatic droplet control and solid-state micromanipulation. This strategy unlocks new technological pathways for intelligent material transport and multifunctional membrane systems, offering a versatile platform for next-generation contact-free manipulation technologies.

2. Results

2.1. Electrostatic tweezer

The TAPA-TFP covalent organic framework (COF) membrane was prepared via an interfacial polymerization (IP) reaction between an aqueous phase and an organic phase [50] (Fig. 1a). Briefly, the organic phase consisted of a dichloromethane solution containing TAPA and TFP, while the water phase contained 3.0 M acetic acid solution. The IP process between the organic and water phases yielded a continuous, uniform, and flexible COF membranes, denoted as TAPA-TFP. The scanning electron microscopy (SEM) (Fig. S1) observation revealed that the membrane surface was smooth and flat, without noticeable defects, pores, or cracks. This continuous structure enables the membrane to maintain flatness and stability when floating on the water surface, providing an ideal kinetic basis for electrostatic manipulation. The elemental analysis (Fig. S2) clearly indicated a homogeneous distribution of C, N, O across the membrane. The X-ray diffraction (XRD) patterns (Fig. S3) showed that the TAPA-TFP membrane possesses good crystallinity, with distinct diffraction peaks at 6.36° and 22.4°, which can be attributed to (001) and (100) plane peaks, respectively, reflecting the highly ordered structure of the membrane framework. The high crystallinity of the membrane ensures mechanical stability and uniform charge distribution during motion. The linkage of TAPA and TFP through β-ketoenamine bonds, as well as the extensive hydrogen bonding within the framework, were revealed by Fourier transform infrared spectroscopy (FTIR) and X-ray photoelectron spectroscopy (XPS) analyses [51–53] (Figs. S4−5). The membrane surface contains oxygen and nitrogen active sites within the β-ketoenamine moieties, which impart a negative charge to the membrane in aqueous solution (zeta potential of −12.2 mV) (Figs. S6−7). This charge characteristic is crucial for the design of the ET, enabling the membrane to efficiently interact with electrostatic forces and achieve remote, contact-free actuation.

To enhance the wide applicability and practicality of the membrane manipulation system, we propose the ET strategy for membrane manipulation, which removes the need for complex electrode arrays and an external power source, enables ultra-flexible and programmable membrane manipulation through electrostatic fields generated by high-voltage-polarized nylon and PTFE control platforms. The design concept of the ET platform, as illustrated in Fig. 1b, includes a control platform and a membrane motion platform. The nylon and PTFE control platforms are pre-charged by high-voltage polarization to generate stable surface charges, serving as the core body of the electrostatic tweezers for remote regulation of the target COF membrane. The operator can control the electric field generated by the ET and enabling remote, contact-

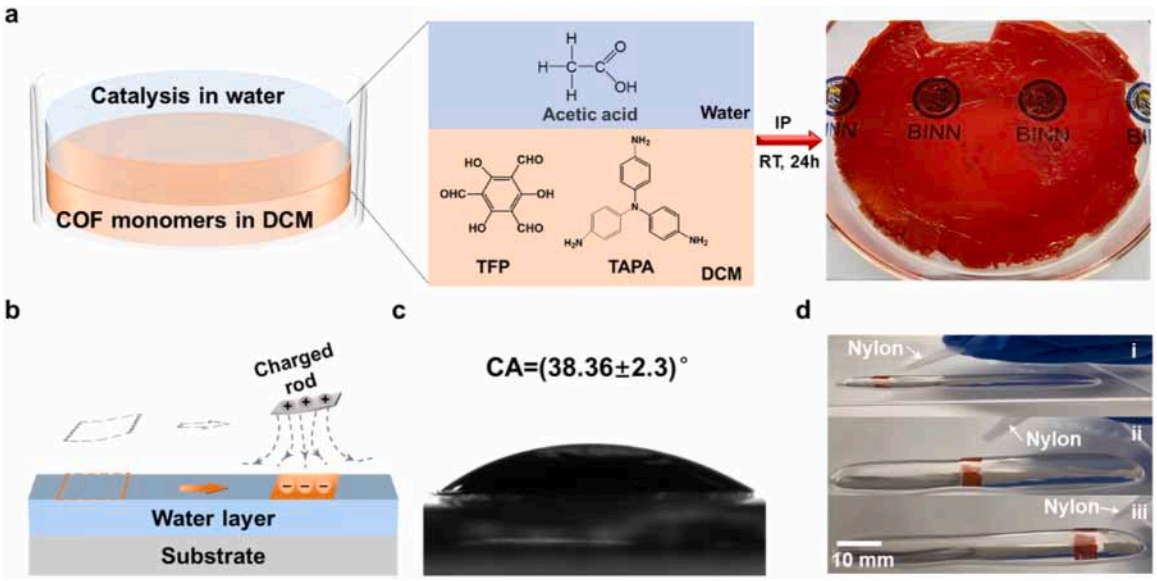


Fig. 1. ET platform and membrane controllability. (a) Schematic illustration and photograph of the interfacial polymerization (IP) process for fabricating TAPA-TFP COF membranes. (b) Schematic of the electrostatic tweezer (ET) including control platform (nylon film) and membrane motion platform (a substrate, a water layer, and a flexible membrane floating on the water layer). (c) Desirable hydrophilicity properties of the TAPA-TFP membrane. (d) Sequential images showing the controllability of the ET.

free, multidirectional actuation of the membrane. The membrane motion platform consists of a substrate, a water layer, and a flexible membrane floating on the water layer. The solid substrate provides stable support for the system, and the layer of water covering it supplies buoyancy and hydrogen bonding to the membrane, reducing frictional resistance and stabilizing its position. This allows the membrane to respond sensitively and rapidly to the electric field while floating on the water surface, enabling flexible, fast, and reversible motion under the action of the electric field, thereby enhancing the membrane manipulation sensitivity and stability in multiple directions. As shown in the atomic force microscopy (AFM) and the cross-sectional SEM image (Figs. S8 9), the TAPA-TFP membrane has a thickness of only 250 nm and exhibits excellent thinness and flexibility, allowing it to float on the water surface without breaking or sinking. This lightweight structure not only reduces the membrane load but also minimizes contact resistance with the water layer, providing favorable conditions for contact-free manipulation. The membrane exhibited a contact angle of 38.36° on water (Fig. 1c), demonstrating excellent hydrophilicity, which facilitates stable spreading on the water surface and enables smooth response to the applied electric field during manipulation.

To clarify the feasibility of the electrostatic tweezer for membrane manipulation, we investigated the effect of different electrostatic forces on the membrane motion on the water surface. As shown in Fig. 1d, and Movie S1, when nylon film was brought near the membrane, the membrane moved rapidly, demonstrating a sensitive response to the electrostatic force and eventually coming to rest at the final position on the water layer. In contrast, when PTFE was brought close to the membrane, the membrane didn't move on the water surface because it carried a negative charge and the direction of the electrostatic force was not sufficiently aligned with the surface charge of the membrane (Fig. S10 and Movie S1). This finding significantly enhanced the controllability of the electrostatic force over the membrane, indicating that programmable control manipulation of the membrane can be achieved by tuning the interaction between the electrostatic polarity generated by the friction materials and the surface charge of the membrane.

Supplementary material related to this article can be found online at doi:10.1016/j.nanoen.2026.112134.

2.2. Multifunctional membrane manipulation

To further demonstrate the dexterous manipulation capabilities of the ET, we move the membrane in diverse complex scenarios, such as being guided following an arbitrary programmed trajectory, achieving membrane capture and release, manipulation in different salt solutions and concentrations, movement under different surface chemical states, testing under varying temperature and humidity conditions, and uphill motion on inclined surfaces. As shown in Fig. 2a, Fig. S11 and Movies S2 3, the membrane moves controllably along the path "ET" and along the trajectories of triangular, square, and circular shapes, demonstrating programmable trajectory controllability and path reproducibility. Trajectory deviations were estimated by manual tracking of membrane position from video recordings. Relative to target trajectories, the membrane exhibits reproducible millimeter-scale path-following fidelity. These results indicate that the ET is able to move the membrane along any programmed path. In addition, the ET al.so enables controlled capture and release of the membrane (Fig. 2b and Movie S4). When the nylon film approaches the membrane, the positive charges on its surface attract the negatively charged membrane, enabling effective capture. Subsequently, the negatively charged PTFE approaches from the back side of the nylon film, weakening or even canceling the nylon's adsorption effect on the membrane. This allows the membrane to detach from the nylon film surface and be released smoothly, achieving a capture and release action similar to that of conventional tweezers. In addition to manipulation on the horizontal dimension, the ET enables membranes to move uphill on inclined surfaces, which is usually highly challenging for conventional manipulation methods. As shown in Fig. 2c, under the action of electrostatic driving force, the membrane can effectively move steadily along a slope with an inclination of 3°, while maintaining a stable posture and a continuous motion trajectory (Movie S5). This performance indicated that ET not only possesses control planar manipulation capability but can also handle complex terrains and multidirectional force fields, enabling flexible application of the membrane in challenging environments.

Supplementary material related to this article can be found online at doi:10.1016/j.nanoen.2026.112134.

The well-controlled membrane manipulation is also demonstrated by the adaptability in various environment conditions. The ET exhibited

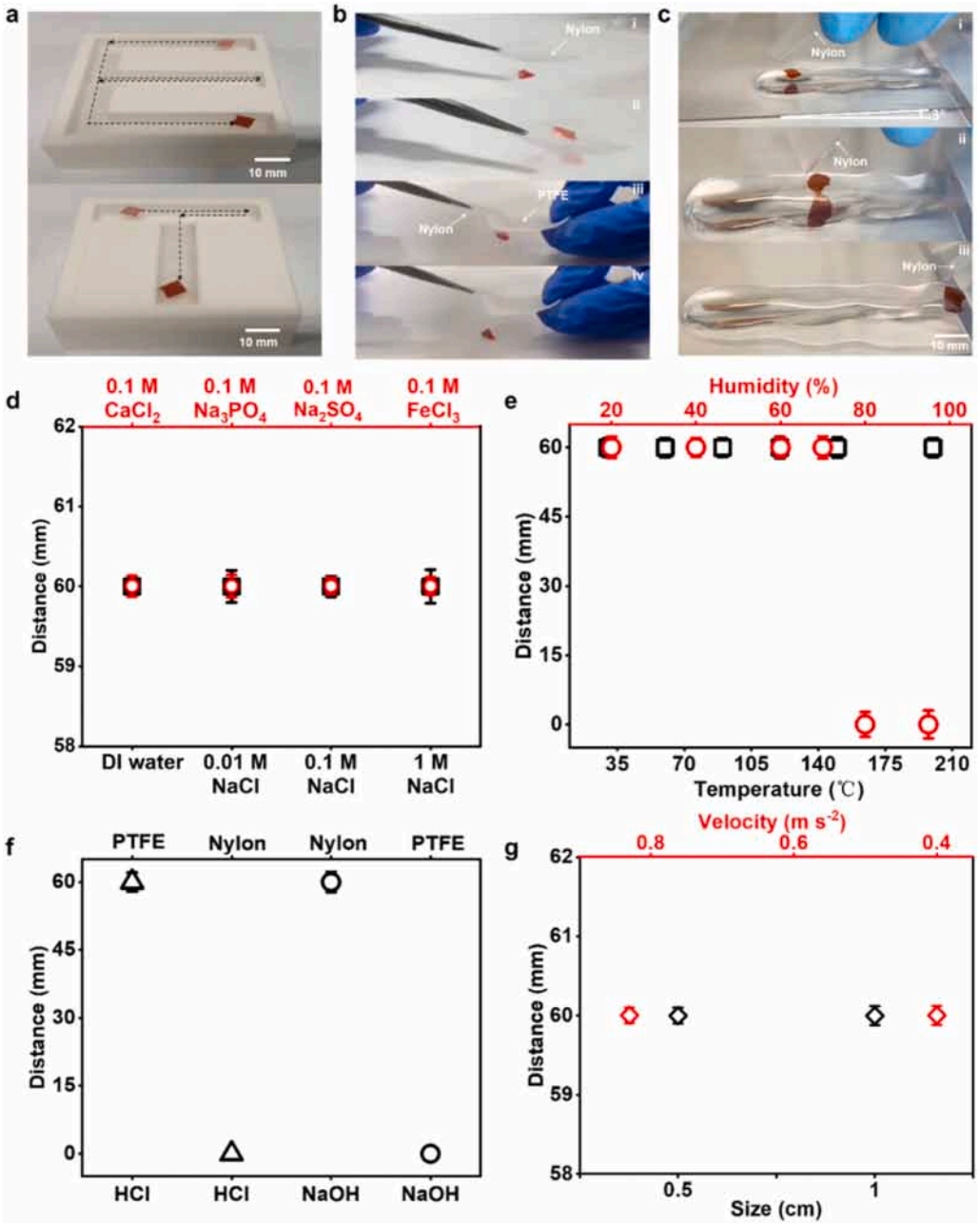


Fig. 2. Multifunctional manipulation of the electrostatic tweezer (ET). (a) Manipulating 5 mm × 5 mm membrane by the ET to move along the preset "ET'' path. (b) Capability of the ET in performing capture and release functions analogous to conventional optical tweezers. (c) Membrane sliding upward along the water surface at a tilt angle of 3°. (d) Generality of membrane transportation for various liquids. The ET shows wide versatility for transporting membrane, including those with types and concentrations of salt solutions, DI water. The error bars in d, e, f, g, and h represent the standard error from three measurements. (e) Capability of the ET in transporting membranes under different air humidity and temperature conditions. (f) Membrane manipulation of corrosive acid and alkali. Nylon film and PTFE film represent two different hand-control platforms. The membrane was immersed in HCl (pH=2) and NaOH (pH=12) solutions. (g) Comparison of distance and velocity between membranes with sizes of 5 mm × 5 mm and 10 mm × 10 mm.

sensitive and controllable motion in NaCl solutions of different concentrations (0.01 M, 0.1 M and 1 M), demonstrating rapid responsiveness and stability (Fig. 2d and Movie S6). Despite the charge-screening effects and interfacial-tension variations associated with 1 M NaCl, reliable membrane manipulation remains achievable. The COF membrane retains sufficient electrostatic responsiveness owing to its intrinsically charged β-ketoenamine framework, while the externally generated electrostatic field remains capable of driving membrane motion despite partial ionic screening. Moreover, the ultrathin hydrophilic membrane remains stably supported at the liquid interface, and the resulting interfacial-tension changes do not preclude electrostatically driven in-plane transport. Furthermore, the ET can be manipulated in various 0.1 M salt solutions ($CaCl_2$, Na_3PO_4, Na_2SO_4, and $FeCl_3$), demonstrating high responsiveness and adjustability across different ionic environments (Fig. 2d and Movie S7). These results highlighted the universal applicability and robustness of the ET across a wide range of salt solution environments, providing a reliable foundation for its use in complex liquid environments. To further evaluate the environmental adaptability of the ET, we also examined the effects of temperature and humidity on membrane motion. For thermal tests, the substrate was preheated at varied temperatures (30 °C, 60 °C, 90 °C, 120 °C, 150 °C, and 200 °C) for 30 min in an oven before adding a thin water layer and

subsequent manipulation. Experimental results showed the membrane maintained stable and responsive motion under such preheated-substrate conditions, demonstrating excellent thermal adaptability of the system (Fig. 2e and Movie S8). However, humidity has a significant impact on membrane manipulation performance. Under low humidity conditions (20%, 40%, 60%, 70% RH), the membrane can move smoothly and respond to the applied electrostatic field, whereas under high humidity conditions (80%, 95% RH), membrane motion is noticeably hindered and manipulation efficiency is significantly reduced (Fig. 2e-f and Movie S9). This may be attributed to the reduced charging efficiency at high humidity, which limits precise controllability of the membrane.

Supplementary material related to this article can be found online at doi:10.1016/j.nanoen.2026.112134.

In addition, we investigated the motion behavior of the membrane under different surface chemical states. As shown in Supplementary Fig. S12 and Movie S10, the membrane placed on HCl or NaOH aqueous layers exhibits actuation under the positively charged nylon film, whereas the negatively charged PTFE induces no response. Specifically, the membrane immersed in an acidic environment (pH = 2, HCl solution) became positively charged (zeta potential 15.75 mV), and the carbonyl and amino groups on its surface form strong hydrogen-bond network with water molecules [51,52] (Fig. S12). Consequently, it was highly responsive to negatively charged PTFE but showed minimal response to positively charged nylon film, allowing PTFE-driven membrane manipulation (Fig. 2f and Movie S11). Conversely, the membrane immersed in an alkaline environment (pH = 12, NaOH solution) became negatively charged (zeta potential −28.87 mV) (Fig. S7), showing sensitivity to positively charged nylon film while remaining unresponsive to negatively charged PTFE, allowing nylon film-driven membrane manipulation (Fig. 2f and Movie S11). These results demonstrate that the ET enables controllable manipulation dictated by the surface chemical state of the membrane. In addition, we investigated the effect of membrane size on its motion behavior. As shown in Fig. 2g and Movie S12, manipulation experiments were conducted on membranes of different sizes under the same electrostatic conditions. The results showed that smaller membranes (5 mm × 5 mm) respond more quickly, whereas larger membranes (10 mm × 10 mm) move slightly slower due to the effects of water surface friction and resistance. These results indicated that membrane size has a significant effect on the response speed of electrostatic manipulation.

Supplementary material related to this article can be found online at doi:10.1016/j.nanoen.2026.112134.

To summarize, the ET not only enables contactless, rapid membrane manipulation in programmable paths on a horizontal water surface but can also achieve several dexterous capabilities including membrane grasping and release, and uphill motion on inclined surfaces. The ET demonstrates the universal adaptability to temperatures, humidity, pH, and electrolyte solution, sustaining reliable manipulation of the membrane in varied chemical and physical environments. As summarized in Table S1, the performance of the present approach is benchmarked against representative droplet-based manipulation strategies across seven key metrics: unlimited distance, unlimited direction, precise stopping, contactless actuation, manipulated target, load-coupled actuation, and metamorphic origami programmability [11,20,21,54], “Y”, “N,” and “NG” in the graph indicate yes, no, and not given in the literature, respectively. Across these dimensions, the membrane manipulation strategy reported here exhibits a distinctly superior overall performance, particularly in enabling long-range transport, accurate positional control, robust contactless operation and versatile metamorphic origami transformations. Remote, reversible and contact-free membrane actuation is realized through electrostatic control, while adaptive motion regulation is further achieved via load-coupled actuation. Notably, this platform extends effective contactless manipulation to charged membranes. Collectively, these attributes substantially outperform existing droplet-based manipulation techniques and establish a new technological paradigm for charged membranes actuation, microdevice transport and reconfigurable functional systems.

2.3. Manipulation mechanism of the ET

To elucidate the mechanism underlying membrane manipulation by ET, the force balance acting on the membrane at the water interface was systematically analysed. Charges accumulated on the nylon film generate a surrounding electrostatic field, as illustrated in Fig. 3a, within which both the electric potential and the field intensity decay progressively with increasing distance from the charged nylon film (Fig. S13). The electrostatic force can be regarded as the resultant of the Maxwell stresses acting on the membrane surface.

The electrostatic force is the sum of the Maxwell stresses acting on the surface of the TAPA-TFP membrane [55,56]:

$$F_e = \oint \left[\varepsilon E(En) - \frac{\varepsilon}{2}E^2 n\right] dS$$

where ε and E are the permittivity of the membrane and the electric field intensity at the TAPA-TFP membrane surface, respectively, and n and S are the surface unit normal and surface area of the TAPA-TFP membrane, respectively. The Coulomb force can be quantified in tensor form [20,24,57]:

$$F_e = \oint T_{e,ij} \bullet n dS, \quad with\ T_{e,\ ij} = \varepsilon_0 \left(E_i E_j - \frac{\delta_{ij}}{2}E^2\right), \quad i,\ \ j = x,\ \ y,\ \ z$$

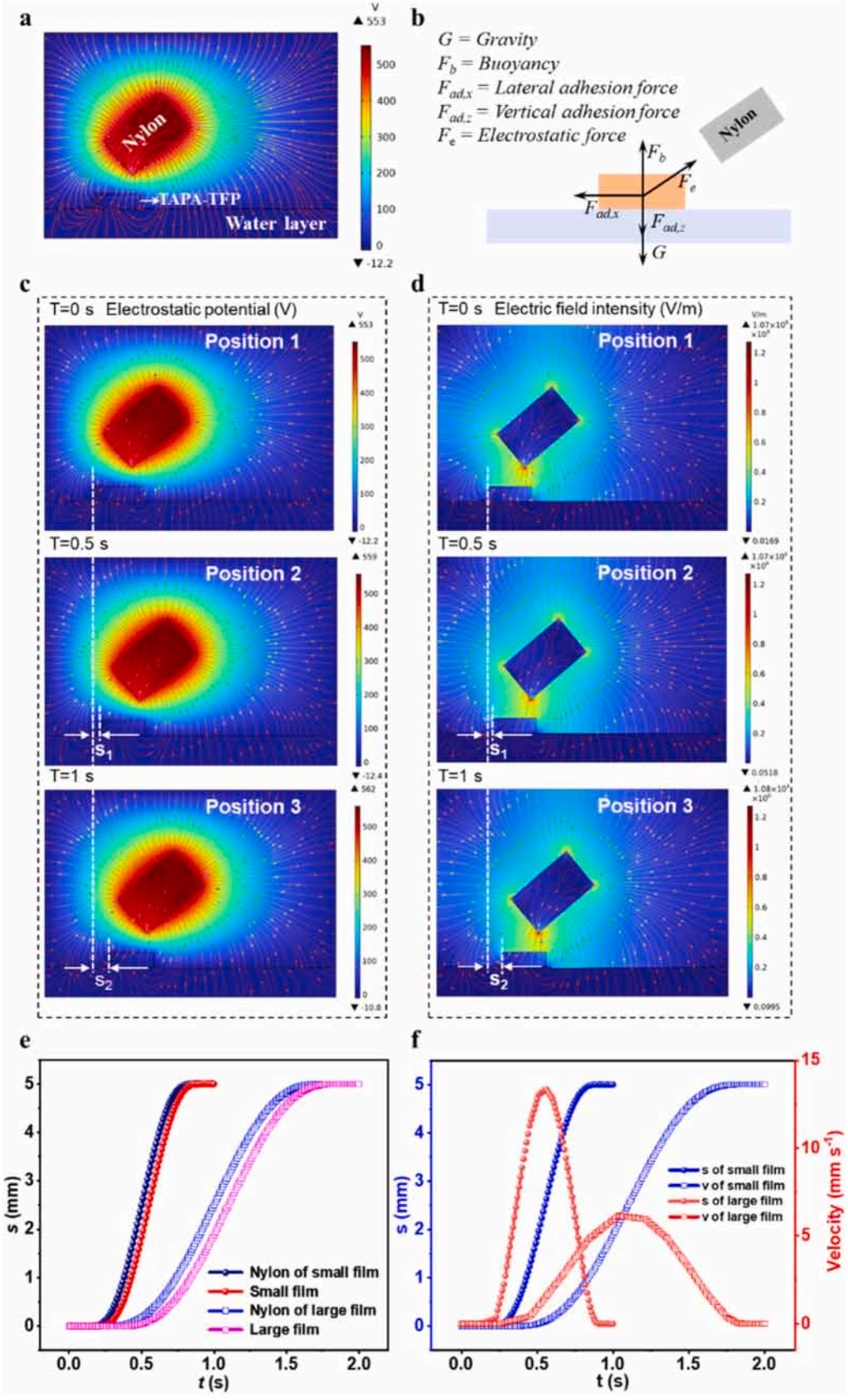
where T_e, n, ε_0, δ_{ij}, and E are the Maxwell stress tensor, surface unit normal vector, the permittivity of air, the Kronecker delta function, and the magnitude of the electric field intensity, respectively. The distribution of T_e on the TAPA-TFP membrane can be calculated via COMSOL-Multiphysics finite-element analysis simulation, as shown in Supplementary Fig. S13. Because the nylon film carries positive charges while the TAPA-TFP membrane is negatively charged, and the electric field intensity associated with the positive charges is stronger than that of the negative charges, the resulting electrostatic force is directed toward the nylon film, thereby providing the driving force for membrane motion.

The dynamic behavior of a TAPA-TFP membrane moving on a water layer is governed by the net force acting on the membrane. Fig. 3b presents the force analysis of the TAPA-TFP membrane under ET manipulation, where the membrane is subjected to the combined effects of electrostatic force (F_e), gravity (G), vertical adhesion force ($F_{ad,z}$, due to hydrogen bond force), lateral adhesion force ($F_{ad,x}$), and buoyancy (F_b). We consider only the lateral manipulation of the membrane. In the vertical direction, the gravity (G), vertical adhesion force ($F_{ad,z}$), buoyancy (F_b), and the vertical component of the electrostatic force (F_e) are balanced, resulting in a net force of zero. The propulsion of the membrane on the water surface is driven by the combined action of the lateral component of the electrostatic force (F_e) and the lateral adhesion force ($F_{ad,x}$). The net driving force F acting on the membrane can be expressed by the following formula [32]:

$$F = F_e \cos\alpha - F_{ad,x}$$

where α is the angle between the electrostatic force and the horizontal direction. This relation provides a fundamental understanding of membrane motion in an electrostatic field. when the ET is close enough to the membrane, $F_e \cos\alpha$ can be greater than $F_{ad,x}$. When $F > 0$, the membrane begins to move, which is driven forward by electrostatic forces. By moving the nylon film and maintaining the proper distance between the nylon film and the membrane, the membrane can be guided to move uniformly on the water surface.

For simplicity, the nylon film and the TAPA-TFP COF membrane can be considered as point charges, and net driving force F_{POINT} can be expressed as follows [54]:



(caption on next page)

Fig. 3. Manipulation mechanism of the electrostatic tweezer (ET). (a) Numerical simulation (based on finite element analysis) of the electric potential distribution around the ET. The colored streamlines represent the electric field lines in space, with arrows indicating the direction of the electric field acting on the TAPA-TFP membrane (5 mm × 5 mm). (b) Force analysis of TAPA-TFP membranes on the water surface under electrostatic interactions. (c), (d) An electrostatic potential (c) and electric field intensity (d) distributions of the TAPA-TFP membrane (5 mm × 5 mm) at three typical positions within the electrostatic field. (e) Calculated displacement (s) of two TAPA-TFP membranes of different sizes (the small membrane: 5 mm × 5 mm, the large membrane: 10 mm × 10 mm) and the target nylon film as a function of time (t). (f) Calculated velocity (v) and displacement (s) of TAPA-TFP membranes (small membrane: 5 mm × 5 mm, large membrane: 10 mm × 10 mm), showing the differences in dynamic response between the two membranes.

$$F_{POINT} = F_{e,POINT}\cos\alpha - F_{ad,x} = \frac{q_1 q_2 \cos\alpha}{4\pi\varepsilon_0\varepsilon_r r^2} - \frac{1}{2}C\rho S v^2$$

where ε_0 is the vacuum permittivity, ε_r is the effective relative permittivity of water, q_1 is the charge on the nylon film, q_2 is the charge on the TAPA-TFP membrane, r is the distance between the TAPA-TFP membrane and the nylon film, ρ represents the density of water, C is the water drag coefficient, S refers to the surface area of the membrane in contact with water, and v indicates the velocity of membrane. To improve both the generality and physical rigor of the model, the TAPA-TFP membrane and the nylon film are treated as objects with well-defined geometries. Under this formulation, the net driving force F acting on the membrane can be expressed as follows:

$$F = F_e\cos\alpha - F_{ad,x} = \int_{V_1}\int_{V_2} \frac{q_{r_1} q_{r_2} \hat{r}_{12}}{4\pi\varepsilon_0\varepsilon_r |r_1 - r_2|^2} dV_1 dV_2 \cos\alpha - \frac{1}{2}C_{eff}\rho S v^2$$

$$F = \frac{\cos\alpha}{4\pi\varepsilon_0\varepsilon_r}\int_{V_1}\int_{V_2} \frac{q_{r_1} q_{r_2} \hat{r}_{12}}{|r_1 - r_2|^2} dV_1 dV_2 - \frac{1}{2}C_{eff}\rho S v^2$$

where q_{r1} and q_{r2} represent the charge quantities at an infinitesimal element of the nylon film and the TAPA-TFP membrane, respectively, $\hat{r}_{12}$denotes the unit vector between the two infinitesimal elements, and $|r_1 - r_2|$ stands for the magnitude of r_{12}. The integration domains V_1 and V_2 correspond to the volumes of the nylon film and the TAPA-TFP membrane, respectively. The water resistance coefficient is replaced by C_{eff}, which is influenced by parameters such as object geometry, surface roughness, and motion state. From this relation, it follows that the net driving force, and hence the actuation performance, decreases with increasing separation between the nylon film and the TAPA-TFP membrane, higher ambient humidity (which accelerates charge dissipation), and larger membrane dimensions. Moreover, at a fixed film-membrane distance, the membrane velocity and the net driving force are mutually constrained, giving rise to an upper limit on the attainable actuation speed. The qualitative dependencies predicted by this model are in strong agreement with the trends observed in both experiments and simulations.

To reveal the driving mechanism of membrane motion, we analyze the electrostatic field distribution using finite element simulations in COMSOL Multiphysics. The configuration of the simulation domain is consistent with the geometry of the ET, and the TAPA-TFP membrane was set in a rectangular to resemble its actual shape geometry in Fig. 1b. Fig. 3c-d show the potential distribution and electric field intensity distribution of the small membrane (5 mm × 5 mm, TAPA-TFP) at three representative positions within the electrostatic field. The colored cloud maps represent the potential and electric field intensity distribution on the nylon film surface, while the colored streamlines represent the electric field lines in space, with arrows indicating the direction of the electric field. Position 1 corresponds to the initial state of membrane motion (T = 0 s), at which the membrane has not yet displaced, and the travel distance is 0. The electrostatic potential distribution shows that the region occupied by the nylon film appears in deep red, corresponding to a high-potential area. The colored streamlines converge from the nylon film toward the membrane, with the electric field lines oriented upward to the right, indicating a substantial electric potential difference between the two materials. This potential difference generates an electrostatic force that initially acts on the membrane in the upward-right direction, consistent with its subsequent motion to the right. The electric field intensity decreases with increasing distance from the nylon film toward the membrane, indicating a corresponding attenuation of the driving force as the separation increases. When the TAPA-TFP membrane begins to move to the right under the driving force of electrostatic attraction and reaches Position 2 (T = 0.5 s), its cumulative travel distance is s_1. During this following-motion stage, the low-potential membrane exhibits a certain response lag as it follows the movement of the high-potential nylon film due to the effects of hydrogen bonding, surface tension, and frictional forces. The resulting change in separation distance causes a variation in the red-to-yellow transition zone between the nylon film and the membrane. This indicates that the electric potential, electrostatic force, and electric field strength distribution acting on the membrane are slightly modified. At T = 1 s, the membrane further moves to Position 3, with the travel distance increasing to s_2. During the movement, the electric potential and field intensity remain basically constant between the nylon film and the membrane, enabling the membrane to experience a strong, stable directional electrostatic driving force under a constant spacing condition, thereby sustaining continuous forward motion (Movies S13−14). Similarly, we also simulated the potential and electric field intensity distributions at three corresponding positions for a large membrane (10 mm × 10 mm) under the same electrostatic field conditions (Fig. S14). The results show that, although the overall potential distribution and field directionality around the large membrane are broadly similar to those of the small membrane, the increased membrane size substantially amplifies the resistive forces associated with membrane-water interfacial tension. Consequently, under the same electrostatic driving force, the balance between driving and resistive forces is shifted, leading to a markedly smaller cumulative displacement of the large membrane at corresponding time points and a significantly attenuated overall dynamic response (Movies S15−16).

Supplementary material related to this article can be found online at doi:10.1016/j.nanoen.2026.112134.

To more intuitively and systematically evaluate the influence of membrane size on electrostatic driving behavior, numerical simulations were performed to model the dynamics of TAPA-TFP membranes under an applied electrostatic field, with the temporal evolution of membrane displacement and velocity quantitatively analyzed. Fig. 3e shows the relationship between displacement (s) and time (t) for two TAPA-TFP membranes of different sizes (5 mm × 5 mm small membrane and 10 mm × 10 mm large membrane) and the target nylon film under the same electrostatic driving force. The results indicate that, from the standpoint of actuation feasibility, TAPA-TFP membranes of both sizes can be displaced under electrostatic forcing, demonstrating the general applicability of this manipulation strategy across different length scales. However, their dynamic responses differ markedly. The larger membrane exhibits a delayed onset of motion and a reduced displacement growth rate relative to the smaller membrane, reflecting a substantial increase in membrane-water interfacial resistance with increasing size, which diminishes electrostatic driving efficiency. By contrast, the smaller membrane experiences lower interfacial resistance, responds more rapidly to the electrostatic force, and displays smoother, more continuous motion, ultimately achieving a higher overall migration velocity. The velocity-time (v–t) profiles (Fig. 3f) quantitatively compare the dynamic responses of membranes with different sizes under electrostatic actuation. The smaller membrane (5 mm × 5 mm) exhibits markedly faster transient kinetics, reaching a peak velocity of

~13.5 mm s^{-1} at ~0.55 s, whereas the larger membrane attains a substantially lower peak velocity of ~6.2 mm s^{-1} with a delayed maximum at ~1.1 s. This contrast indicates that the smaller membrane experiences higher instantaneous acceleration and a more agile dynamic response. Consistently, within the same 1 s time window, its velocity remains significantly higher than that of the larger membrane. Experimentally, the measured peak velocities are ~10 mm s^{-1} for the small membrane and ~5.6 mm s^{-1} for the large membrane, slightly lower than the simulated values. This discrepancy arises from unavoidable experimental factors, including hydrodynamic dissipation, interfacial disturbances, and measurement uncertainty. Moreover, the electrostatic charge on the nylon film was not optimized to its theoretical maximum, as experimental charge densities are lower than the ideal values assumed in simulations. Consequently, the experimentally observed velocities do not represent the intrinsic upper performance limit of the system. Overall, the numerical simulations are in excellent agreement with both theoretical predictions and experimental observations. Consistent conclusions emerge from analytical derivation, numerical simulation, and experiment: increasing membrane size reduces the net driving force, thereby degrading actuation performance. Conversely, under identical driving conditions, reducing the membrane size markedly enhances electrostatic driving efficiency, enabling faster and more stable motion. This pronounced size effect establishes a clear physical basis for optimizing the dynamic performance of electrostatically driven membranes.

To elucidate the influence of environmental humidity on electrostatically driven TAPA-TFP membranes, we performed numerical simulations to analyze their motion under varying humidity conditions. Figs. S15a-b show the potential distribution cloud maps under low-humidity conditions, while Figs. S15c-d correspond to the electric field intensity distributions. Figs. S15e-f present the potential distribution cloud maps under high-humidity conditions (≥85%), and Figs. S15g-h correspond to the electric field intensity distributions under high humidity. In both low-and high-humidity cases, the initial position of the left end of the membrane remains the same, i.e., at $t = 0$ s, $x_{10} = x_{20}$. Under low-humidity conditions, the potential distribution at $t = 0$ s reveals a pronounced electric potential difference between the nylon film and the membrane, accompanied by substantial electric field intensity. At $t = 1$ s, both the potential and field intensity slightly decrease, but a significant field gradient remains, allowing the membrane to stably follow the charged nylon film, with its left end reaching x_{11}. In contrast, under high-humidity conditions, the initial potential and field distributions are similar, but by $t = 1$ s, high-potential regions weaken markedly, and the electric field intensity around the membrane is substantially reduced, with the gradient nearly disappearing. Consequently, the membrane barely displaces with the nylon film, reaching only x_{21}. The difference in displacement can be expressed quantitatively as $\Delta s = x_{11} - x_{21}$. This behavior arises because high humidity accelerates dissipation of electrostatic charges on the nylon film surface, weakening the potential and electric field and thus reducing the electrostatic driving force. These simulation results align closely with theoretical analysis and experimental observations, demonstrating that increased humidity accelerates charge dissipation, lowers net driving force, and diminishes actuation performance. Therefore, maintaining a low-humidity environment is essential for effective electrostatic actuation. In summary, theoretical, simulation, and experimental results all show consistent qualitative trends regarding the impact of humidity on driving performance.

In addition, we further performed simulations to investigate how different surface chemical states of TAPA-TFP membranes affect their electrostatic response and resultant motion. The results show that when the membrane is immersed in HCl solution (pH 2), it becomes positively charged. In the nylon system (Fig. S16a, $t = 0$ s), both the membrane and nylon film carry positive charges. By $t = 1$ s (Fig. S16b), no significant potential gradient forms, and the membrane shows zero displacement, indicating that a positively charged nylon film cannot drive a positively charged membrane. In contrast, in the PTFE system (Figs. S16c-d), the membrane is positive while PTFE is negative. By $t = 1$ s, a clear potential gradient develops, driving effective membrane displacement (Δs_1), demonstrating that negatively charged PTFE can electrostatically drive a positively charged membrane. Conversely, when the membrane is immersed in NaOH solution (pH 12), it becomes negatively charged. In the nylon system (Figs. S16e-f), the membrane and positively charged nylon film form a pronounced potential gradient, resulting in effective displacement (Δs_2). In the PTFE system (Figs. S16g-h), both surfaces are negatively charged, no gradient forms, and the membrane shows negligible motion. These simulation results closely match experimental observations, confirming that the membrane's surface chemical state critically regulates electrostatic driving. Moreover, they demonstrate that the ET system provides excellent selective control over membrane motion, establishing a foundation for controllable electrostatic manipulation across multiple systems.

Building on the aforementioned analysis, we further validated the feasibility and programmability of this electrostatic manipulation strategy in complex three-dimensional environments. The results show that the system can stably drive the membrane along predetermined trajectories, including "E" and "T" shaped paths (Movies S17), accurately reproducing complex routes with turns and branches, which demonstrates excellent directional switching and path-following stability. Moreover, by constructing regular geometric trajectories, the membrane can execute closed-loop motion along square or triangular paths (Movies S18). These three-dimensional simulations confirm that the strategy is effective not only for linear or planar motion but also for manipulation along complex spatial paths, highlighting its outstanding spatial adaptability and trajectory programmability. Such capabilities provide a solid foundation for potential applications in microstructured environments, reconfigurable systems, and spatially constrained platforms.

Supplementary material related to this article can be found online at doi:10.1016/j.nanoen.2026.112134.

2.4. Multifunctional applications of the ET

Building on the capabilities demonstrated in Fig. 4, the ET enables a set of application scenarios that are difficult to access with existing manipulation paradigms, encompassing directional motion guidance, load-coupled actuation, metamorphic origami remote control and operation within enclosed environments. As shown in Fig. 4a, the TAPA-TFP membrane can be guided through a maze-like trajectory under the electrostatic attraction induced by the charged nylon film actuator, illustrating deterministic navigation along complex paths with high positional fidelity (Movie S19). This capability highlights the potential of the ET for programmable motion guidance and trajectory planning in constrained geometries. Beyond locomotion, the ET supports load-coupled actuation and controlled cargo transport. As illustrated in Fig. 4b, a 5 mm × 5 mm membrane (0.04 mg) loaded with methylene red powder (1 mg) can be remotely translated to designated locations without mechanical contact, demonstrating its function as a mobile carrier for reagent delivery (Movie S20). This mode of operation underscores the feasibility of using flexible membranes as multifunctional platforms that integrate actuation and payload transport, with implications for microdelivery systems and lab-on-chip technologies [58]. The ET further enables dynamic shape reconfiguration of flexible membranes. As shown in Fig. 4c, a folded membrane undergoes rapid unfolding and controlled deformation under electrostatic guidance, achieving remote metamorphic origami remote control (Movie S21). This capability reflects the controllability with which the ET can regulate both translational motion and structural transformation, pointing towards applications in bioinspired metamorphic robotics and reconfigurable devices where shape adaptation is integral to function [59]. Importantly, the electrostatic control strategy allows fully contact-free manipulation within enclosed systems. Fig. 4d demonstrates the

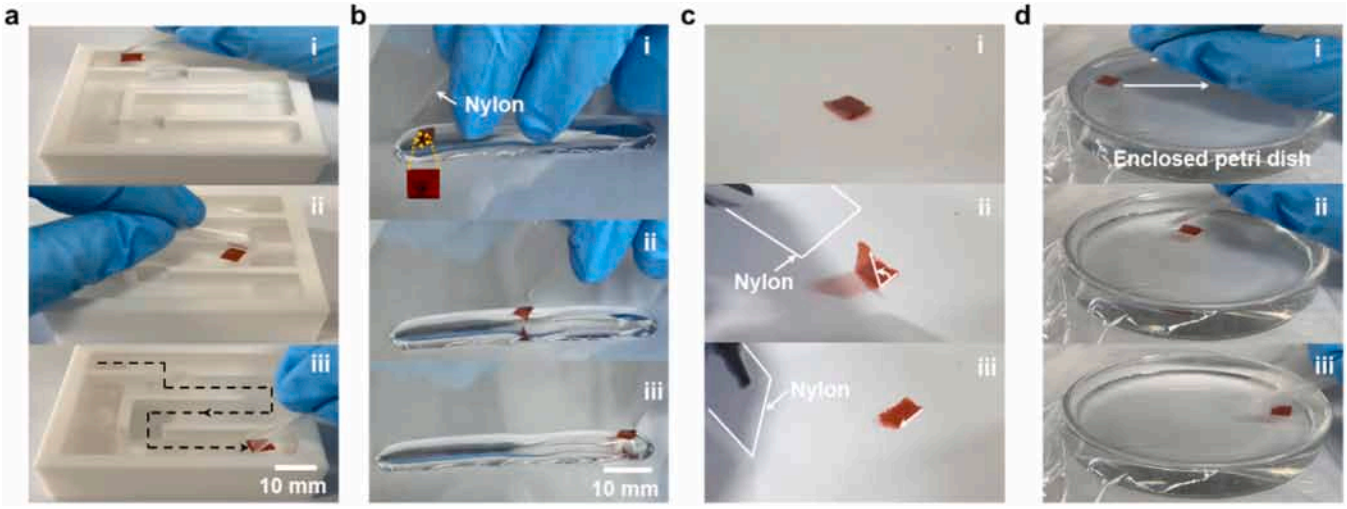


Fig. 4. The applications of the electrostatic tweezer (ET). (a) The ET navigation of a membrane through a maze. (b) Load-coupled actuation application of the ET using a 5 mm × 5 mm membrane. The inset shows the membrane loaded with methylene red powder. (c) Metamorphic origami control application of the ET using a 5 mm × 10 mm membrane. Folded COF membrane is placed on dry substrate, gradual unfolding is actively triggered and controlled by remote electrostatic field. (d) Manipulating a membrane in a closed Petri dish from the outside.

remote actuation of the TAPA-TFP membrane inside a sealed Petri dish driven entirely by external electrostatic fields (Movie S22). This feature is particularly relevant for biosafe, contamination-sensitive or chemically isolated environments, where direct mechanical access is undesirable or impractical [60].

Supplementary material related to this article can be found online at doi:10.1016/j.nanoen.2026.112134.

More broadly, the electrostatic field-based control paradigm presented here represents one of the few approaches capable of systematically approaching the long-standing objective of remote manipulation with high-dimensional trajectory control, uphill motion on inclined surfaces and complex shape reconfiguration. Beyond its immediate functional advantages, this strategy resonates with emerging directions in materials science, flexible electronics and control theory, where field-driven responses are increasingly exploited to transcend the limitations of contact-based actuation [61]. In this context, remote and contact-free control evolves from a means of orchestrating motion into a foundational capability for regulating the movement, morphology and functionality of matter itself. Control is no longer confined to mechanical interfaces or structural constraints, but enters a regime in which energy fields, particularly electrostatic fields, directly govern material response [62–64]. Solid materials thus transition from passive structural elements to dynamic carriers that can be remotely activated, reconfigured and programmed. By unifying complex motion, uphill motion on inclined surfaces and shape reconfiguration within macroscopic solid systems, electrostatic control establishes a general and scalable framework for controllable manipulation, with profound implications for intelligent materials, operation in closed environments and, the realization of programmable matter [65,66].

3. Conclusion

Remote, contact-free manipulation of solid matter has remained a long-standing challenge, with existing strategies largely limited to droplets, rigid particles, or micromechanical components. Here, we introduce an electrostatic driven ET platform that achieves controllable, programmable, and omnidirectional control of charged membranes without physical contact, embedded electrodes, or external power. By harnessing electrostatic fields generated by nylon films, intrinsically charged TAPA-TFP membranes can be guided along arbitrary two- and three-dimensional trajectories, uphill motion on inclined surfaces, reconfigured into complex metamorphic origami states, and used for load-coupled transport. Unlike conventional droplet-based electrostatic actuation, this approach integrates high-speed motion (with peak velocities approaching 10 mm s^{-1}), shape morphing, and selective capture-release within a single framework, operating robustly across wide ranges of pH, humidity, temperature, surface chemistry, and electrolyte composition. This work establishes a generalizable paradigm for through-air electrostatic actuation of charged membranes at air-liquid interface.

CRediT authorship contribution statement

Di Wei: Writing – review & editing, Funding acquisition, Conceptualization. **Zhong Lin Wang:** Conceptualization. **Zhe Wang:** Funding acquisition, Conceptualization. **Zhongqiang Zhang:** Writing – review & editing, Conceptualization. **Ziyang Wang:** Writing – review & editing, Software. **Lixue Yang:** Writing – review & editing, Writing – original draft, Software, Formal analysis, Data curation, Conceptualization. **Zunkang Zhou:** Data curation. **Jie Fu:** Data curation. **Yu Wei:** Formal analysis.

Declaration of Competing Interest

The authors declare that they have no known competing financial interests or personal relationships that could have appeared to influence the work reported in this paper.

Acknowledgement

We acknowledge financial support from the National Natural Science Foundation (grant number 22479016, U24A20505, and 52473205).

Appendix A. Supporting information

Supplementary data associated with this article can be found in the

online version at doi:10.1016/j.nanoen.2026.112134.

Data availability

The data that has been used is confidential.

References

[1] S. Ham, J.S. Popovics, Application of contactless ultrasound toward automated inspection of concrete structures, Autom. Constr. 58 (2015) 155–164, https://doi.org/10.1016/j.autcon.2015.07.018.

[2] W. Zhou, P. Xiao, Y. Liang, Q. Wang, D. Liu, Q. Yang, J. Chen, Y. Nie, S.-W. Kuo, T. Chen, Bionic adaptive thin-membranes sensory system based on microspring effect for high-sensitive airflow perception and noncontact manipulation, Adv. Funct. Mater. 31 (2021) 2105323, https://doi.org/10.1002/adfm.202105323.

[3] X. Li, Y. Guo, C. Li, Y. Zhang, Y. Zheng, R. Wang, X. Yu, W. Ding, Q. Tong, Recent advances in cutaneous haptic interfaces: a review, SmartSys 2 (2026) e70018, https://doi.org/10.1002/sys3.70018.

[4] M. Abdelgawad, A.R. Wheeler, The Digital Revolution: A new paradigm for microfluidics, Adv. Mater. 21 (2009) 920–925, https://doi.org/10.1002/adma.200802244.

[5] Z. Shen, D. Zhu, M. Zhang, Synergy of smart materials and structures toward intelligent metamaterials, SmartSys 1 (2025) e70007, https://doi.org/10.1002/sys3.70007.

[6] I. Hajji, M. Serra, L. Geremie, I. Ferrante, R. Renault, J.L. Viovy, S. Descroix, D. Ferraro, Droplet microfluidic platform for fast and continuous-flow RT-qPCR analysis devoted to cancer diagnosis application, Sens. Actuators B Chem. 303 (2020) 127171, https://doi.org/10.1016/j.snb.2019.127171.

[7] G. Shim, S. Ko, D. Kim, Q.-V. Le, G.T. Park, J. Lee, T. Kwon, H.-G. Choi, Y.B. Kim, Y.-K. Oh, Light-switchable systems for remotely controlled drug delivery, J. Control. Release 267 (2017) 67–79, https://doi.org/10.1016/j.jconrel.2017.09.009.

[8] G.J. Shah, A.T. Ohta, E.P.Y. Chiou, M.C. Wu, C.-J.C. Kim, EWOD-driven droplet microfluidic device integrated with optoelectronic tweezers as an automated platform for cellular isolation and analysis, Lab. a Chip 9 (2009) 1732–1739, https://doi.org/10.1039/B821508A.

[9] W. Wang, H. Vahabi, A. Taassob, S. Pillai, A.K. Kota, On-demand, contact-less and loss-less droplet manipulation via contact electrification, Adv. Sci. 11 (2024) 2308101, https://doi.org/10.1002/advs.202308101.

[10] L. Lu, C. Jiang, G. Hu, J. Liu, B. Yang, Noncontact sensing: flexible noncontact sensing for human–machine interaction, Adv. Mater. 33 (2021) 2170125, https://doi.org/10.1002/adma.202170125.

[11] Z. Yuan, C. Lu, C. Liu, X. Bai, L. Zhao, S. Feng, Y. Liu, Ultrasonic tweezer for multifunctional droplet manipulation, Sci. Adv. 9 (2023) eadg2352, https://doi.org/10.1126/sciadv.adg2352.

[12] Y. Xiao, S. Zarghami, K. Wagner, P. Wagner, K.C. Gordon, L. Florea, D. Diamond, D. L. Officer, Moving droplets in 3D using light, Adv. Mater. 30 (2018) 1801821, https://doi.org/10.1002/adma.201801821.

[13] C. Haber, D. Wirtz, Magnetic tweezers for DNA micromanipulation, Rev. Sci. Instrum. 71 (2000) 4561–4570, https://doi.org/10.1063/1.1326056.

[14] A.F. Demirörs, S. Aykut, S. Ganzeboom, Y.A. Meier, E. Poloni, Programmable droplet manipulation and wetting with soft magnetic carpets, Proc. Natl. Acad. Sci. 118 (2021) e2111291118, https://doi.org/10.1073/pnas.2111291118.

[15] W. Yan, C. Zhao, W. Luo, W. Zhang, X. Li, D. Liu, Optically guided pyroelectric manipulation of water droplet on a superhydrophobic surface, ACS Appl. Mater. Interfaces 13 (2021) 23181–23190, https://doi.org/10.1021/acsami.1c03407.

[16] X. Tang, L. Wang, Loss-free photo-manipulation of droplets by pyroelectro-trapping on superhydrophobic surfaces, ACS Nano 12 (2018) 8994–9004, https://doi.org/10.1021/acsnano.8b02470.

[17] M.A. Ghanem, A.D. Maxwell, Y.-N. Wang, B.W. Cunitz, V.A. Khokhlova, O. A. Sapozhnikov, M.R. Bailey, Noninvasive acoustic manipulation of objects in a living body, Proc. Natl. Acad. Sci. 117 (2020) 16848–16855, https://doi.org/10.1073/pnas.2001779117.

[18] D. Foresti, M. Nabavi, M. Klingauf, A. Ferrari, D. Poulikakos, Acoustophoretic contactless transport and handling of matter in air, Proc. Natl. Acad. Sci. 110 (2013) 12549–12554, https://doi.org/10.1073/pnas.1301860110.

[19] T. Sneh, S. Corsetti, M. Notaros, K. Kikkeri, J. Voldman, J. Notaros, Optical tweezing of microparticles and cells using silicon-photonics-based optical phased arrays, Nat. Commun. 15 (2024) 8493, https://doi.org/10.1038/s41467-024-52273-x.

[20] Y. Jin, W. Xu, H. Zhang, R. Li, J. Sun, S. Yang, M. Liu, H. Mao, Z. Wang, Electrostatic tweezer for droplet manipulation, Proc. Natl. Acad. Sci. 119 (2022) e2105459119, https://doi.org/10.1073/pnas.2105459119.

[21] Q. Sun, D. Wang, Y. Li, J. Zhang, S. Ye, J. Cui, L. Chen, Z. Wang, H.-J. Butt, D. Vollmer, X. Deng, Surface charge printing for programmed droplet transport, Nat. Mater. 18 (2019) 936–941, https://doi.org/10.1038/s41563-019-0440-2.

[22] J. Nie, Z. Ren, J. Shao, C. Deng, L. Xu, X. Chen, M. Li, Z.L. Wang, Self-powered microfluidic transport system based on triboelectric nanogenerator and electrowetting technique, ACS Nano 12 (2018) 1491–1499, https://doi.org/10.1021/acsnano.7b08014.

[23] J. Li, C.-J.C. Kim, Current commercialization status of electrowetting-on-dielectric (EWOD) digital microfluidics, Lab. a Chip 20 (2020) 1705–1712, https://doi.org/10.1039/D0LC00144A.

[24] W. Xu, Y. Jin, W. Li, Y. Song, S. Gao, B. Zhang, L. Wang, M. Cui, X. Yan, Z. Wang, Triboelectric wetting for continuous droplet transport, Sci. Adv. 8 (2022) eade2085, https://doi.org/10.1126/sciadv.ade2085.

[25] G. Zhou, A. Yang, Y. Wang, G. Gao, A. Pei, X. Yu, Y. Zhu, L. Zong, B. Liu, J. Xu, N. Liu, J. Zhang, Y. Li, L.-W. Wang, H.Y. Hwang, M.L. Brongersma, S. Chu, Y. Cui, Electrotunable liquid sulfur microdroplets, Nat. Commun. 11 (2020) 606, https://doi.org/10.1038/s41467-020-14438-2.

[26] J. Yu, X. Wei, Y. Guo, Z. Zhang, P. Rui, Y. Zhao, W. Zhang, S. Shi, P. Wang, Self-powered droplet manipulation system for microfluidics based on triboelectric nanogenerator harvesting rotary energy, Lab. a Chip 21 (2021) 284–295, https://doi.org/10.1039/D0LC00994F.

[27] J. Nie, T. Jiang, J. Shao, Z. Ren, Y. Bai, M. Iwamoto, X. Chen, Z.L. Wang, Motion behavior of water droplets driven by triboelectric nanogenerator, Appl. Phys. Lett. 112 (2018) 183701, https://doi.org/10.1063/1.5030152.

[28] G. Chen, X. Liu, S. Li, M. Dong, D. Jiang, A droplet energy harvesting and actuation system for self-powered digital microfluidics, Lab. a Chip 18 (2018) 1026–1034, https://doi.org/10.1039/C7LC01259D.

[29] J. Xu, Z. Lei, J. Guo, J. Huang, W. Wang, U. Reibetanz, S. Xu, Trapping and driving individual charged micro-particles in fluid with an electrostatic device, Nano-Micro Lett. 8 (2016) 270–281, https://doi.org/10.1007/s40820-016-0087-3.

[30] J. Sun, L. Zhang, S. Gong, J. Chen, H. Guo, Mechano-driven tribo-electrophoresis enabled human–droplet interaction in 3D space, Adv. Mater. 35 (2023) 2305578, https://doi.org/10.1002/adma.202305578.

[31] R. Li, X. Li, Z. Zhang, M. Willatzen, Z.L. Wang, D. Wei, Triboelectric programmed droplet manipulation for plug-and-play assembly, Adv. Funct. Mater. 35 (2025) 2416457, https://doi.org/10.1002/adfm.202416457.

[32] J. Yong, X. Li, Y. Hu, Y. Peng, Z. Cheng, T. Xu, C. Wang, D. Wu, Triboelectric 'electrostatic tweezers' for manipulating droplets on lubricated slippery surfaces prepared by femtosecond laser processing, Int. J. Extrem. Manuf. 6 (2024) 035002, https://doi.org/10.1088/2631-7990/ad2cdf.

[33] J. Yong, X. Li, Y. Hu, Y. Wang, Y. Peng, Z. Chen, Y. Zhang, S. Zhu, C. Wang, D. Wu, Portable triboelectric electrostatic tweezer for external manipulation of droplets within a closed femtosecond laser-treated superhydrophobic system, Nano Lett. 24 (2024) 7116–7124, https://doi.org/10.1021/acs.nanolett.4c01953.

[34] C. Liu, F. Wang, X. Du, Self-powered electrostatic tweezer for adaptive object manipulation, Device 2 (2024) 100465, https://doi.org/10.1016/j.device.2024.100465.

[35] M. McEvoy, N. Correll, Materials science. Materials that couple sensing, actuation, computation, and communication, Science (New York N. Y.) 347 (2015) 1261689, https://doi.org/10.1126/science.1261689.

[36] X. Hu, T. Tan, Y. Chen, Z. Yan, Spatially programmable origami networks enable high-density mechanical computing for autonomous robotics, Nat. Commun. 16 (2025) 10209, https://doi.org/10.1038/s41467-025-64956-0.

[37] W. Yan, S. Li, M. Deguchi, Z. Zheng, D. Rus, A. Mehta, Origami-based integration of robots that sense, decide, and respond, Nat. Commun. 14 (2023) 1553, https://doi.org/10.1038/s41467-023-37158-9.

[38] A. Sharma, S. Naskar, T. Mukhopadhyay, Multi-physically programmable tubular origami metamaterials: exploitable nexus of geometry, folding mechanics and stimuli-responsive physics, Adv. Sci. 12 (2025) e05089, https://doi.org/10.1002/advs.202505089.

[39] L. Yang, L.N.Y. Cao, S. Li, P. Peng, H. Qian, G. Amaratunga, F. Yang, Z.L. Wang, D. Wei, MOFs/MXene nano-hierarchical porous structures for efficient ion dynamics, Nano Energy 129 (2024) 110076, https://doi.org/10.1016/j.nanoen.2024.110076.

[40] L. Yang, S. Li, H. Qian, Z. Wang, Z.L. Wang, D. Wei, Osmotic power generation based on nanoconfined materials, MRS Energy Sustain. 11 (2024) 193–218, https://doi.org/10.1557/s43581-024-00104-3.

[41] L. Yang, Z. Wang, Z.L. Wang, D. Wei, Porous organic framework membranes with nanostructures for osmotic power conversion, water desalination, and selective separation, ChemNanoMat 11 (2025) e202400629, https://doi.org/10.1002/cnma.202400629.

[42] Y. Su, H. Peng, X. Liu, J. Li, Q. Zhao, High performance, pH-resistant membranes for efficient lithium recovery from spent batteries, Nat. Commun. 15 (2024) 10295, https://doi.org/10.1038/s41467-024-54503-8.

[43] D. Wei, IONTRONICS inaugural editorial: defining a new frontier with iontronics, Iontronics 1 (2025) 1, https://doi.org/10.20517/iontronics.2025.01.

[44] X. Li, Z.L. Wang, D. Wei, Iontronic logic control driven by dynamic electrical double layer regulation, Iontronics 1 (2025) 2, https://doi.org/10.20517/iontronics.2025.02.

[45] Z. Li, Z. Guo, F. Zhang, L. Sun, H. Luan, Z. Fang, J.L. Dedrick, Y. Zhang, C. Tang, A. Zhu, Y. Yu, S. Ding, D. Wang, A.-Y. Chang, L. Yin, L.M. Russell, W. Gao, R. H. Fang, L. Zhang, J. Wang, Inhalable biohybrid microrobots: a non-invasive approach for lung treatment, Nat. Commun. 16 (2025) 666, https://doi.org/10.1038/s41467-025-56032-4.

[46] Y.-H. Huang, M.-J. Wang, T.-S. Chung, Development of multifunctional membranes via plasma-assisted nonsolvent induced phase separation, Nat. Commun. 15 (2024) 1092, https://doi.org/10.1038/s41467-024-45414-9.
[47] J. Kim, P. Mayorga-Burrezo, S.-J. Song, C.C. Mayorga-Martinez, M. Medina-Sánchez, S. Pané, M. Pumera, Advanced materials for micro/nanorobotics, Chem. Soc. Rev. 53 (2024) 9190–9253, https://doi.org/10.1039/D3CS00777D.
[48] Q. Gao, M. Kim, D. von Arx, E. Zhang, X. Zhang, H. Ye, C. Vogt, C. Ehmke, D. Corsino, F. Catania, N. Münzenrieder, M. Magno, G. Cantarella, B.J. Nelson, S. Pané, Soft magnetic microrobots with remote sensing and communication capabilities, Nat. Commun. 16 (2025) 10489, https://doi.org/10.1038/s41467-025-65459-8.
[49] Y. Sun, B. Sun, X. Cui, W. Li, Y. Zhang, L. He, S. Nong, Z. Zhu, J. Wu, D. Li, X. Li, S. Zhang, X. Li, M. Li, Addressable and perceptible dynamic reprogram of ferromagnetic soft machines, Nat. Commun. 16 (2025) 2267, https://doi.org/10.1038/s41467-025-57454-w.
[50] J. Liu, G. Han, D. Zhao, K. Lu, J. Gao, T.-S. Chung, Self-standing and flexible covalent organic framework (COF) membranes for molecular separation, Sci. Adv. 6 (2020) eabb1110, https://doi.org/10.1126/sciadv.abb1110.
[51] J.L. Segura, M.J. Mancheño, F. Zamora, Covalent organic frameworks based on Schiff-base chemistry: synthesis, properties and potential applications, Chem. Soc. Rev. 45 (2016) 5635–5671, https://doi.org/10.1039/C5CS00878F.
[52] S. Kandambeth, K. Dey, R. Banerjee, Covalent organic frameworks: chemistry beyond the structure, J. Am. Chem. Soc. 141 (2019) 1807–1822, https://doi.org/10.1021/jacs.8b10334.
[53] W. Tang, J. Zeng, F. Bian, H. Lin, H. Zhao, Z.-Y. Lu, Engineering heteroatomic structures in Pt single-atom anchored covalent organic frameworks for enhanced photocatalytic hydrogen evolution reaction, J. Mater. Chem. A 13 (2025) 19682–19694, https://doi.org/10.1039/D5TA01922B.
[54] J. Sun, Q. Zhao, Z. Mo, J. Chen, H. Guo, L. Zhang, Self-powered droplet manipulation for full human-droplet interaction in multiple mediums, Nat. Commun. 16 (2025) 2312, https://doi.org/10.1038/s41467-025-57656-2.
[55] F. Wang, F. Guo, Z. Wang, H. He, Y. Sun, W. Liang, B. Yang, Surface charge density gradient printing to drive droplet transport: a numerical study, Langmuir 38 (2022) 13697–13706, https://doi.org/10.1021/acs.langmuir.2c01772.
[56] D.R. Link, E. Grasland-Mongrain, A. Duri, F. Sarrazin, Z. Cheng, G. Cristobal, M. Marquez, D.A. Weitz, Electric control of droplets in microfluidic devices, Angew. Chem. Int. Ed. 45 (2006) 2556–2560, https://doi.org/10.1002/anie.200503540.
[57] Y. Jin, X. Liu, W. Xu, P. Sun, S. Huang, S. Yang, X. Yang, Q. Wang, R.H.W. Lam, R. Li, Z. Wang, Charge-powered electrotaxis for versatile droplet manipulation, ACS Nano 17 (2023) 10713–10720, https://doi.org/10.1021/acsnano.3c01919.
[58] H.G. Shin, W.K. Chung, K. Kim, Soft and flexible robot skin actuator using multilayer 3D pneumatic network, Nat. Commun. 16 (2025) 5575, https://doi.org/10.1038/s41467-025-60496-9.
[59] Y. Li, A. Di Lallo, J. Zhu, Y. Chi, H. Su, J. Yin, Adaptive hierarchical origami-based metastructures, Nat. Commun. 15 (2024) 6247, https://doi.org/10.1038/s41467-024-50497-5.
[60] S. Yuan, C. Xu, B. Cui, T. Zhang, B. Liang, W. Yuan, H. Ren, Motor-free telerobotic endomicroscopy for steerable and programmable imaging in complex curved and localized areas, Nat. Commun. 15 (2024) 7680, https://doi.org/10.1038/s41467-024-51633-x.
[61] P. Jiao, J. Mueller, J.R. Raney, X. Zheng, A.H. Alavi, Mechanical metamaterials and beyond, Nat. Commun. 14 (2023) 6004, https://doi.org/10.1038/s41467-023-41679-8.
[62] X. Huang, X. Xiang, C. Li, J. Nie, Y. Shao, Z. Xu, Q. Zheng, Electrostatic in-plane structural superlubric actuator, Nat. Commun. 16 (2025) 493, https://doi.org/10.1038/s41467-024-55078-0.
[63] R. Zhang, Triboelectric Intelligence, SmartSys 1 (2025) e2, https://doi.org/10.1002/sys3.2.
[64] Y. Li, Y. Luo, S. Xiao, C. Zhang, C. Pan, F. Zeng, Z. Cui, B. Huang, J. Tang, T. Shao, X. Zhang, J. Xiong, Z.L. Wang, Visualization and standardized quantification of surface charge density for triboelectric materials, Nat. Commun. 15 (2024) 6004, https://doi.org/10.1038/s41467-024-49660-9.
[65] Y. Jung, K. Kwon, J. Lee, S.H. Ko, Untethered soft actuators for soft standalone robotics, Nat. Commun. 15 (2024) 3510, https://doi.org/10.1038/s41467-024-47639-0.
[66] T. Jin, Z. Sun, L. Li, Q. Zhang, M. Zhu, Z. Zhang, G. Yuan, T. Chen, Y. Tian, X. Hou, C. Lee, Triboelectric nanogenerator sensors for soft robotics aiming at digital twin applications, Nat. Commun. 11 (2020) 5381, https://doi.org/10.1038/s41467-020-19059-3.



Lixue Yang achieved the M.S. degree from the Henan Normal University in 2023. She continues pursing Ph.D. degree in Changchun University of Technolog, and is jointly trained by the Beijing Institute of Nanoenergy and Nanosystems, Chinese Academy of Sciences. Her research focuses on the transformation of ions and electrons, with applications in osmotic energy harvesting.



Ziyang Wang, PhD student at the School of Mechanical Engineering, Jiangsu University. He has published 3 academic papers, has 2 invention patents, has presided over 1 provincial-level project, has participated in 1 provincial-level project, has received one first prize and one third prize in provincial-level innovation competitions, and has received several university-level awards, etc.



Zunkang Zhou is currently a PhD candidate at Beijing Institute of Nanoenergy and Nanosystems, Chinese Academy of Sciences. His research focuses on the electrical double layer at solid-liquid interfaces.



Yu Wei achieved his B.S. degree from Tianjin University of Science and Technology in 2023. He is pursuing an Ph.D. degree at the Beijing Institute of Nanoenergy and Nanosystems. His research interests include the electrical double layer at solid-liquid contact electrification interfaces.



Jie Fu has over 14 years of experience in the R&D, manufacturing, and marketing of new material products, transformation of scientific and technological achievements, and investment and financing. Currently serving as the Director of the Product Development Center at Zhejiang Wansheng Co., Ltd., he is responsible for the incubation, business development, and market expansion of polymer additives and special polymer resins, as well as the establishment of an open innovation ecosystem for fine chemical materials. Based on hands-on practical experience, he has developed a comprehensive understanding of the new materials industry at the macro, meso, and micro levels, with profound expertise in business development collaboration, product development, corporate operations, and capital management.



Zhongqiang Zhang, professor, Dean of the School of Mechanical Engineering, Jiangsu University, Doctor of Engineering from Dalian University of Technology, visiting scholar at the University of California, Berkeley, director of the Micro-nano Devices and Systems Technology Division of the China Instrument and Control Society, member of the Computational Mechanics Committee of the Jiangsu Society of Theoretical and Applied Mechanics, member of the Energy Structure Mechanics Committee of the Jiangsu Society of Theoretical and Applied Mechanics, international advisor for IOP journals, editorial board member of Mechanical Design and Manufacturing Engineering, youth editorial board member of Advanced Manufacturing, etc. He has presided over 5 projects of the National Natural Science Foundation of China, 1 sub-project of the "Co-existing Robotics" Major Research Plan Integration Project of the National Natural Science Foundation of China, 1 sub-project of the National Key Research and Development Program of the Ministry of Science and Technology of China, undertaken 4 key projects including national defense, Jiangsu Provincial Industrial Foresight, and the Provincial Agricultural Committee's funded innovation, and presided over more than 10 provincial and ministerial level projects. He has published over 100 SCI-indexed papers in internationally renowned journals in his field such as Science Advances, AFM, Nano Energy, Chemical Engineering Journal, with over 1300 citations. He has written 1 English monograph, and been granted more than 20 invention patents. He has received the First Prize of Jiangsu Provincial Science and Technology Award, the 2023 ICCES Outstanding Young Scholar Award, etc.



Prof. **Zhe Wang** is a doctoral supervisor at Changchun University of Technology, currently serving as the dean of the College of Chemistry and Life Sciences. His research focuses on the molecular design, structure, morphology, and transport mechanisms of polymer membrane materials. During his research career, he has published over 100 SCI-indexed papers in important academic journals, which have been cited more than 1000 times. He has received two provincial and ministerial second-class awards as the first principal investigator and holds 16 authorized national invention patents. He has led three National Natural Science Foundation general projects, the Ministry of Education's New Century Talent Program, the "Changbai Mountain Scholar" distinguished professor reward program, and over 20 other provincial and ministerial projects, including those funded by Jilin Province's talent development fund, leading talent and project teams, major projects from the Jilin Provincial Department of Science and Technology, the Jilin Provincial Natural Science Foundation, and the Jilin Provincial Development and Reform Commission. Details can be found at: https://www.x-mol.com/groups/wang_zhe



Prof. **Zhong Lin Wang** received his Ph.D. from Arizona State University in physics. He now is the Hightower Chair in Materials Science and Engineering, Regents' Professor, Engineering Distinguished Professor and Director, Center for Nanostructure Characterization, at Georgia Tech. Dr. Wang has made original and innovative contributions to the synthesis, discovery, characterization and understanding of fundamental physical properties of oxide nanobelts and nanowires, as well as applications of nanowires in energy sciences, electronics, optoelectronics and biological science. His discovery and breakthroughs in developing nanogenerators established the principle and technological road map for harvesting mechanical energy from environment and biological systems for powering personal electronics. His research on self-powered nanosystems has inspired the worldwide effort in academia and industry for studying energy for micro-nano-systems, which is now a distinct disciplinary in energy research and future sensor networks. He coined and pioneered the field of piezotronics and piezophototronics by introducing piezoelectric potential gated charge transport process in fabricating new electronic and optoelectronic devices. Details can be found at: http://www.nanoscience.gatech.edu.



Di Wei received his B.Sc. from the University of Science and Technology of China (USTC) and both his M.Sc. and Ph.D. from Åbo Akademi University in Finland. His research focuses on the applications of nanotechnology in energy and sensor systems. In this field, he has published over 120 papers in leading journals, including Nat. Energy, Nat. Commun., Sci. Adv., PNAS, Joule, Matter, Adv. Mater., Angew. Chem. Int. Ed., J. Am. Chem. Soc., Energ. Environ. Sci., Chem. Soc. Rev. etc. Wei holds a portfolio of over 200 international patents (including PCT filings), with nearly 100 successfully granted. Many of these patents have been transferred to leading companies such as Nokia in Finland and Lyten in the USA. Additionally, he has edited four English books published by Wiley and Cambridge University Press, among others. His contributions have been recognized with numerous accolades, including the First Prize of the Nokia Global Innovation and Excellence Award, the Brian Conway Prize in Physical Electrochemistry from the International Society of Electrochemistry (ISE), and various honors from ISE and the Royal Society of Chemistry (RSC). Details can be found at: http://www.iontronics.group/en/